Journal of
Materials Chemistry C

Accepted Manuscript

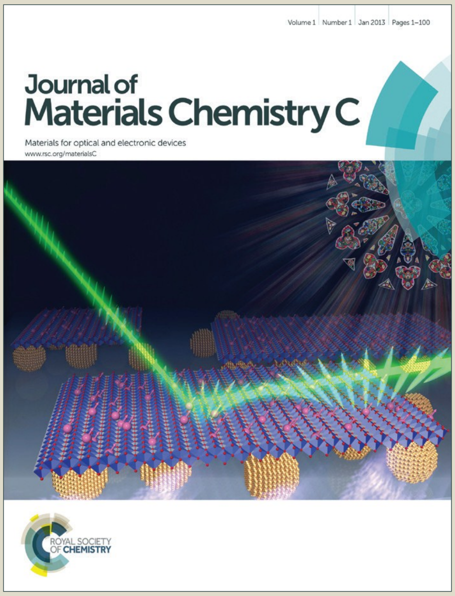

This is an *Accepted Manuscript*, which has been through the Royal Society of Chemistry peer review process and has been accepted for publication.

Accepted Manuscripts are published online shortly after acceptance, before technical editing, formatting and proof reading. Using this free service, authors can make their results available to the community, in citable form, before we publish the edited article. We will replace this *Accepted Manuscript* with the edited and formatted *Advance Article* as soon as it is available.

You can find more information about *Accepted Manuscripts* in the Information for Authors.

Please note that technical editing may introduce minor changes to the text and/or graphics, which may alter content. The journal's standard Terms & Conditions and the Ethical guidelines still apply. In no event shall the Royal Society of Chemistry be held responsible for any errors or omissions in this *Accepted Manuscript* or any consequences arising from the use of any information it contains.

ROYAL SOCIETY
OF CHEMISTRY

www.rsc.org/materialsC

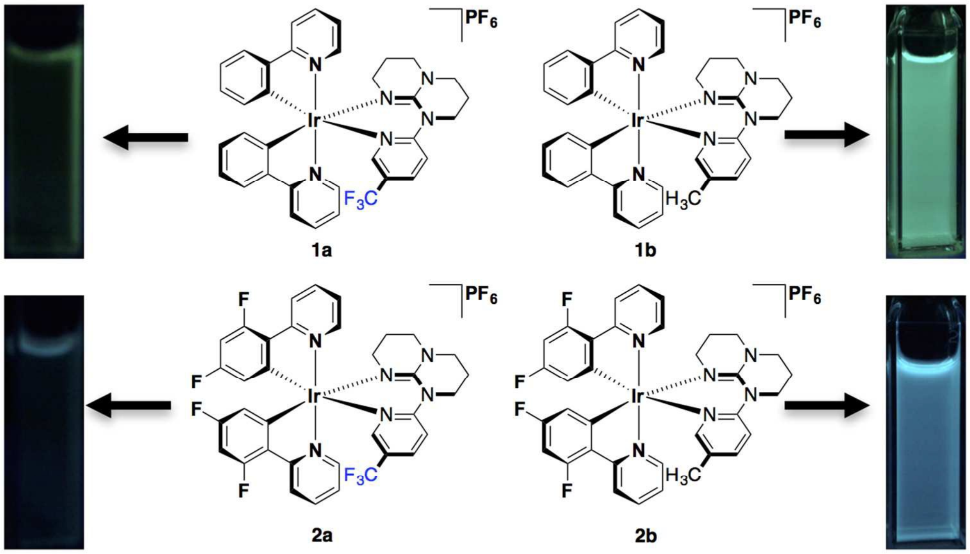
PF$_6$
Ir
N
F$_3$C
H$_3$C
F
1a
1b
2a
2b

Journal Name

ARTICLE

Controlling the Emission Efficiency of Blue-Green Iridium(III) Phosphorescent Emitters and Applications in Solution-Processed Organic Light-Emitting Diodes

Received 00th January 20xx,
Accepted 00th January 20xx

DOI: 10.1039/x0xx00000x

www.rsc.org/

Muhammad T. Sajjad,[a] Nidhi Sharma,[a,b] Amlan K. Pal,[b] Kamrul Hasan,[c,d] Guohua Xie,[a] Lisa S. Kölln,[a] Garry S. Hanan*,[c] Ifor D. W. Samuel*[a] and Eli Zysman-Colman*[b]

We show that the emission efficiency of blue-green phosphorescent emitters can be controlled through coupling of the excited state to vibrational modes. We controlled this vibrational coupling through choice of different ligands and as a result, complexes with CF_3-groups on the ancillary ligand were essentially non-emissive (Φ_{PL} < 1%), whereas with isosteric CH_3-groups the complexes were strongly emissive (Φ_{PL} > 50%). Emission of the complexes can be drastically improved (30 times higher Φ_{PL} compared to degassed solution for the CF_3-containing complexes) by blending them with an inert solid host such as PMMA, which mitigates metal-ligand vibrations. Solution-processed organic light-emitting diodes made from these materials showed efficiency as high as 6.3%.

---

[a] *Organic Semiconductor Centre, SUPA, School of Physics and Astronomy, University of St. Andrews, St. Andrews, Fife, KY16 9SS, UK.*
[b] *Organic Semiconductor Centre, EaStCHEM School of Chemistry, University of St Andrews, St Andrews, Fife, KY16 9ST, UK.*
[c] *Département de Chimie, Université de Montréal, 2900 Edouard-Montpetit, Montréal, Québec H3T-1J4, Canada.*
[d] *Current address: Department of Chemistry, College of Sciences, University of Sharjah, P.O. Box 27272, Sharjah, United Arab Emirates.*

.

Electronic Supplementary Information (ESI) available: [details of any supplementary information available should be included here]. See DOI: 10.1039/x0xx00000x

Journal Name

ARTICLE

Introduction

Iridium complexes have attracted significant attention as potent emitters in organic light-emitting diodes (OLEDs)[1-3] and light-emitting electrochemical cells (LEECs),[4-7] which are electroluminescent devices targeted for next generation flat panel displays and solid-state lighting. This is due to their high photoluminescence quantum yield (Φ_{PL}) and short radiative lifetime, facile colour tunability across the entirety of the visible spectrum, and good thermal and photo stability.[8] Importantly, both singlet and triplet excitons in these complexes contribute to device efficiencies,[9-12] which enables them to attain nearly 100% internal quantum efficiency.[13]

However, the reported OLEDs based on iridium complexes can in many cases show low device efficiency due to rapid non-radiative decay.[10,14,15] One reason for the reduced efficiencies observed is due to enhanced coupling of the excited state to vibrational modes.[10,14-16] Many different methods such as controlling isomer geometry or using rigid structures including inert hosts like poly(methylmethacrylate) (PMMA) and poly(styrene) have been reported for controlling the magnitude of vibrational coupling, which lead to moderate improvement of the quantum yield.[1,17] However, in order to establish a structure-property relationship for achieving both high Φ_{PL} and device efficiency, detailed photophysical and device studies on structurally related complexes are required. Here we show that blue-green cationic iridium(III) complexes of the form $[Ir(C^\wedge N)_2(N^\wedge N)]PF_6$ with the same cyclometallating, C^N, ligands but with different saturated strongly-donating guanidylpyridine (gpy) N^N ligands[18] can be used to control the emission efficiency. We find that there is severe quenching of PL in complexes with a CF_3 on the gpy ligand in solution, which we attribute to vibrational coupling. We show that this can be overcome by embedding the complex in an inert matrix. Therefore, we embedded the complexes within PMMA and observed a significant enhancement of the Φ_{PL} and emission lifetime, τ_e, compared to degassed MeCN solution. Quenching was further reduced at lower temperature. The devices fabricated using solution processing in a multilayer structure show efficiency of more than 6%.

Experimental

Materials and methods

Commercial chemicals were used as supplied. All reactions were performed using standard Schlenk techniques under inert (N_2) atmosphere with freshly obtained anhydrous solvents obtained from a Pure MBRAUN (MB-SPS) purification system except where specifically mentioned. Flash column chromatography was performed using silica gel (Silia-P from Silicycle, 60 Å, 40-63 µm). Analytical thin layer chromatography (TLC) was performed with silica plates with aluminum backings (250 µm with indicator F-254). Compounds were visualized under UV light. ^1H, ^{19}F and ^{13}C NMR spectra were recorded on a Brucker Avance 400 spectrometer at 400 MHz, 376 MHz and 100 MHz, respectively. The following abbreviations have been used for multiplicity assignments: "s" for singlet, "d" for doublet, "t" for triplet, "m" for multiplet and "br" for broad. Deuterated chloroform ($CDCl_3$), and deuterated acetonitrile (CD_3CN) were used as the solvent of record. Chemical shifts are reported in parts per million (ppm) relative to residual solvent ^1H resonance (1.96 ppm for CD_3CN, 7.26 ppm for $CDCl_3$) and the ^{13}C resonance (0.73 ppm and 118.69 ppm for CD_3CN, 77.00 ppm for $CDCl_3$) of the solvent. Melting points (Mp's) were recorded using open-ended capillaries on a Meltemp melting point apparatus and are uncorrected. High-resolution mass spectra were recorded on a quadrupole time-of-flight (ESI-Q-TOF), model MICROTOF II from Bruker in positive electrospray ionization mode at the Université de Montreal. 1,3,4,6,7,8-Hexahydro-2H-pyrimido[1,2-*a*]pyrimidine (H-hpp), 2-bromo-5-(trifluoromethyl)pyridine, 2-bromo-5-methylpyridine, (±) BINAP, $Pd(OAc)_2$, *t*-BuOK were purchased from Aldrich and used as received. The corresponding iridium(III) dimers, $[Ir(C^\wedge N)_2Cl]_2$ were prepared according to the literature, where C^N is 2-phenylpyridinato (ppy) or 2-(4,6-difluorophenyl)-5-methylpyridinato (dFMeppy).[19]

Synthetic details

2,3,4,6,7,8-hexahydro-1-(5-methylpyridin-2-yl)-pyrimido[1,2-a]pyrimidine (Guanidyl-5-methyl-pyridine ***(Me-gpy) L1****)*: An oven-dried two-necked round bottomed flask was charged with (±)-BINAP (0.06 mmol, 0.038 g) and filled with nitrogen followed by multiple vacuum and then added 3 mL dry toluene to make a suspension of BINAP. The resulting suspension was heated at 90 °C for 5 min to dissolve the BINAP. This mixture was cooled to room temperature, $Pd(OAc)_2$ (0.04 mmol, 0.009 g) was added, and the mixture was stirred for 3 min. To the resulting bright yellow solution were added 2- bromo-5-methylpyridine (4 mmol, 0.688 g) and 1,3,4,6,7,8-hexahydro-2*H*-pyrimido[1,2-*a*]pyrimidine (4.3 mmol, 0.600 g) and stirred for 5 min at ambient temperature. The mixture turned into bright orange colour, to which was added *t*-BuOK (5.6 mmol, 0.640 g) and the flask was again charged with nitrogen followed by couple of vacuum. The reaction mixture was then stirred at 90 °C for 5 h, after which time it was cooled to room temperature and diethyl ether (60 mL) was added and the solution was filtered. Evaporation of the filtrate gave the ligand as a yellow oil liquid. Yield: 0.80 g (87%). The synthetic method was adopted from our previously reported protocol.[20] **^1H NMR (400 MHz, Chloroform-d) δ (ppm):** 8.07 (dd, *J* =1.6, 0.8 Hz, 1H), 7.51 (d, *J* = 8.5 Hz, 1H), 7.31 (dd, *J* = 2.4, 8.5 Hz, 1H), 3.82 (m, 2H), 3.39 (m, 2H), 3.22 (t, *J* = 6.1 Hz, 2H), 3.18 (t, *J* = 6.4 Hz, 2H), 2.21 (s, 3H), 2.03 (m, 2H), 1.86 (dd, *J* = 5.8, 11.7

Hz, 2H). **^{13}C NMR (101 MHz, Chloroform-d) δ (ppm):** 155.06, 150.39, 147.17, 137.26, 126.57, 119.30, 49.16, 48.91, 44.39, 44.21, 23.94, 23.08, 18.04. **HR-MS (ES-Q-TOF):** $[M]^+$ ($C_{13}H_{18}N_4$) calculated: 230.1531; experimental: 230.1528.

1-(5-(trifluoromethyl)pyridin-2-yl)-2,3,4,6,7,8-hexahydro-pyrimido[1,2-a]pyrimidine (Guanidyl-5-trifluoromethyl-pyridine ***(CF$_3$-gpy) L2****)*: Yield: 0.50 g (88%). The synthesis was carried out followed by the above method. **^{1}H NMR (400 MHz, Chloroform-d) δ (ppm):** 8.46 (d, *J* =0.8 Hz, 1H), 7.86 (d, *J* =9.0 Hz, 1H), 7.62 (dd, *J* = 2.5, 9.0 Hz, 1H), 3.96 (m, 2H), 3.45 (t, *J* = 5.7 Hz, 2H), 3.26 (t, *J* = 5.9 Hz, 2H), 3.20 (t, *J* = 6.3 Hz, 2H), 2.03 (m, 2H), 1.91 (m,2H). **^{19}F NMR (376 MHz, Chloroform-d) δ (ppm)**: -71.67. **^{13}C NMR (101 MHz, Chloroform-d) δ (ppm)**: 158.77, 149.43, 144.74, 144.69, 132.96, 117.00, 48.95, 48.80, 44.12, 43.41, 23.95, 22.80. **HR-MS (ES-Q-TOF):** $[M+H]^+$ ($C_{13}H_{16}F_3N_4$) calculated: 285.1329; experimental: 285.1323.

General procedure for the synthesis of [Ir(C^N)$_2$(N^N)]PF$_6$ complexes. Iridium dimer (0.07 mmol, 1.0 equiv.) and N^N ligand (Me-gpy or CF$_3$-gpy) (0.15 mmol, 2.10 equiv.) were solubilized with 20 mL of DCM/MeOH (50:50, v/v). The mixture was degassed by multiple vacuum and N_2 purging cycles. The suspension was heated at 50 °C for 19 h. The reaction mixture was cooled to room temperature and evaporated to dryness. The resulting solid was dissolved in a minimum amount of MeOH and a solution of NH_4PF_6 (10 equiv., 1.0 g / 10 mL) was added drop by drop to the methanolic solution to cause the precipitation of a solid. The suspension was cooled to 0 °C for 1 h, filtered and the resulting solid was washed with cold water. The crude solid was purified by flash chromatography on silica gel using DCM to DCM/Acetone (9/1, v/v).

[Ir(ppy)$_2$(CF$_3$-gpy)]PF$_6$, ***1a***. Light Yellow solid. Yield: 0.083 g (71 %). **Mp:** 179 °C. R$_f$: 0.25 (5% DCM/acetone on silica. **^{1}H NMR (400 MHz, Acetonitrile-*d$_3$*) δ (ppm):** 8.59 (d, *J* = 5.8 Hz, 1H), 8.27 (d, *J* = 6.0 Hz, 1H), 8.12 (t, *J* = 7.8 Hz, 3H), 7.97 (q, *J* = 7.8 Hz, 2H), 7.84 (s, 1H), 7.74 (dd, *J* = 16.0, 7.9 Hz, 2H), 7.56 (d, *J* = 9.0 Hz, 1H), 7.32 (t, *J* = 6.4 Hz, 1H), 7.26 (t, *J* = 6.7 Hz, 1H), 6.94 (dd, *J* = 15.6, 7.9 Hz, 2H), 6.80 (dt, *J* = 14.4, 7.4 Hz, 2H), 6.24 (d, *J* = 7.5 Hz, 1H), 6.16 (d, *J* = 7.6 Hz, 1H), 3.83 (m, 1H), 3.41 (m, 2H), 3.38 (m, 1H), 3.21 (m, 1H), 3.07 (dd, *J* = 10.9, 6.2 Hz, 2H), 2.85 (d, *J* = 13.3 Hz, 1H), 2.30 (m, 1H), 2.22 (s, 1H), 1.58 (d, *J* = 5.3 Hz, 1H), 1.15 (m, 1H). **^{19}F NMR (376 MHz, Acetonitrile-*d$_3$*) δ (ppm):** -63.45, -72.00, -73.87. **^{13}C NMR (101 MHz, Acetonitrile-*d$_3$*) δ (ppm):** 168.20, 157.86, 153.21, 152.34, 150.84, 149.68, 147.04, 145.05, 144.69, 138.90, 138.60, 136.92, 132.39, 132.15, 130.22, 129.97, 125.25, 124.58, 123.30, 122.99, 122.43, 122.12, 120.18, 119.88, 48.95, 48.60, 48.24, 46.86, 22.64. **HR-MS (ES-Q-TOF):** $[M-PF_6]^+$ ($C_{35}H_{31}F_3N_6Ir^+$) calculated: 785.2188; experimental: 785.2235.

[Ir(ppy)$_2$(Me-gpy)]PF$_6$, ***1b***. Light yellow solid. Yield: 0.089 g (74%). **Mp:** 164-165 °C. R$_f$: 0.20 (5% DCM/acetone on silica. **^{1}H NMR (400 MHz, Acetonitrile-*d$_3$*) δ (ppm):** 8.64 (d, *J* = 5.8 Hz, 1H), 8.36 (d, *J* = 5.4 Hz, 1H), 8.24 (d, *J* = 8.1 Hz, 1H), 8.19 (d, *J* = 8.1 Hz, 1H), 8.06 (t, *J* = 7.8 Hz, 2H), 7.90 (d, *J* = 7.8 Hz, 1H), 7.82 (dd, *J* = 13.1, 8.2 Hz, 2H), 7.50 (d, *J* = 8.5 Hz, 1H), 7.40 (d, *J* = 11.7 Hz, 2H), 7.33 (d, *J* = 7.0 Hz, 1H), 7.03 (dd, *J* = 17.5, 7.6 Hz, 2H), 6.89 (d, *J* = 6.3 Hz, 2H), 6.34 (d, *J* = 7.6 Hz, 1H), 6.25 (d, *J* = 7.5 Hz, 1H), 3.91 (d, *J* = 13.7 Hz, 1H), 3.53 (d, *J* = 18.9 Hz, 1H), 3.47 (m, 1H), 3.40 (m, 1H), 3.32 (m, 1H), 3.23 (m, 2H), 3.13 (d, *J* = 5.5 Hz, 1H), 3.03 (s, 1H), 2.38 (m, 1H), 2.05 (s, 3H), 1.61 (m, 1H), 1.13 (d, *J* = 5.3 Hz, 1H). **^{13}C NMR (101 MHz, Acetonitrile-*d$_3$*) δ (ppm):** 168.30, 153.91, 153.43, 153.14, 151.16, 150.84, 150.54, 149.07, 144.91, 141.26, 138.56, 138.29, 132.30, 131.72, 129.95, 125.32, 124.33, 123.10, 122.78, 121.92, 120.14, 119.65, 117.19, 48.79, 48.64, 48.33, 46.66, 22.96, 22.86, 16.80. **HR-MS (ES-Q-TOF):** $[M-PF_6]^+$ ($C_{35}H_{34}N_6Ir^+$) calculated: 731.2470; experimental: 731.2494.

[Ir(dFMeppy)$_2$(CF$_3$-gpy)]PF$_6$, ***2a***. Light red solid. Yield: 0.082 g (80%). **Mp:** 193 °C. R$_f$: 0.32 (5% DCM/acetone on silica. **^{1}H NMR (400 MHz, Acetonitrile-*d$_3$*) δ (ppm):** 8.38 (s, 1H), 8.27 (m, 2H), 8.18 (m, 2H), 7.88 (d, *J* = 8.2 Hz, 2H), 7.64 (m, 2H), 6.58 (dtd, *J* = 12.1, 9.6, 2.2 Hz, 2H), 5.76 (dd, *J* = 8.7, 2.3 Hz, 1H), 5.60 (dd, *J* = 8.9, 2.3 Hz, 1H), 3.85 (m, 1H), 3.42 (m, 2H), 3.28 (m, 1H), 3.21 (m, 1H), 3.16 (m, 1H), 3.09 (m, 1H), 2.86 (d, *J* = 13.2 Hz, 1H), 2.39 (s, 3H), 2.38 (s, 3H), 2.31 (m, 1H), 2.22 (m, 1H), 1.67 (s, 1H), 1.15 (t, *J* = 7.0 Hz, 1H). **^{19}F NMR (376 MHz, Acetonitrile-*d$_3$*) δ (ppm):** -64.60, -73.12 (m), -75.01, -110.57 (m), -110.93 (q, *J* = 9.3 Hz), -111.98 (t, *J* = 11.4 Hz), -112.93 (m). **^{13}C NMR (101 MHz, Acetonitrile-*d$_3$*) δ (ppm):** 157.69, 152.50, 151.27, 150.93, 146.94, 140.53, 140.38, 137.54, 134.40, 134.14, 123.56, 123.31, 123.09, 122.90, 118.51, 114.66, 114.43, 98.58, 98.37, 98.24, 98.03, 48.96, 48.62, 48.22, 47.22, 22.74, 22.62, 17.74, 17.34. **HR-MS (ES-Q-TOF):** $[M-PF_6]^+$ ($C_{37}H_{31}F_7N_6Ir^+$) calculated: 885.2124; experimental: 885.2258.

[Ir(dFMeppy)$_2$(Me-gpy)]PF$_6$, ***2b***. Lemon yellow solid. Yield: 0.097 g (81%). **Mp:** 180 °C. R$_f$: 0.22 (5% DCM/acetone on silica. **^{1}H NMR (400 MHz, Acetonitrile-*d$_3$*) δ (ppm):** 8.34 (s, 1H), 8.31 (d, *J* = 8.7 Hz, 1H), 8.23 (d, *J* = 9.5 Hz, 1H), 8.13 (s, 1H), 7.86 (s, 2H), 7.78 (d, *J* = 6.7 Hz, 1H), 7.43 (d, *J* = 8.5 Hz, 1H), 7.17 (s, 1H), 6.55 (dtd, *J* = 12.0, 9.5, 2.3 Hz, 2H), 5.74 (dd, *J* = 8.8, 2.3 Hz, 1H), 5.56 (dd, *J* = 8.9, 2.3 Hz, 1H), 3.82 (d, *J* = 13.5 Hz, 1H), 3.41 (m, 1H), 3.28 (d, *J* = 10.9 Hz, 1H), 3.23 (d, *J* = 9.0 Hz, 1H), 3.18 (dd, *J* = 7.5, 4.5 Hz, 2H), 3.14 (d, *J* = 9.6 Hz, 1H), 3.04 (m, 1H), 2.88 (d, *J* = 13.1 Hz, 1H), 2.37 (s, 3H), 2.36 (s, 3H), 2.28 (d, *J* = 4.5 Hz, 1H), 1.99 (s, 3H), 1.61 (m, 1H), 1.05 (m, 1H). **^{19}F NMR (376 MHz, Acetonitrile-*d$_3$*) δ (ppm):** -73.16, -75.04, -111.10 (q, *J* = 9.4 Hz), -111.38 (q, *J* = 9.4 Hz), -111.98 (m), -113.33 (m). **^{13}C NMR (101 MHz, Acetonitrile-*d$_3$*) δ** (ppm): 161.80, 157.86, 154.72, 153.65, 152.94, 151.31, 150.57, 149.10, 141.79, 140.16, 140.01, 134.01, 133.79, 132.29, 123.57, 123.38, 122.91, 122.71, 114.28, 114.11, 98.20, 97.95, 97.68, 48.80, 48.61, 48.32, 46.87, 30.36, 22.98, 17.88, 17.41, 16.83. **HR-MS (ES-Q-TOF):** $[M-PF_6]^+$ ($C_{37}H_{34}F_4N_6Ir^+$) calculated: 831.2407; experimental: 831.2514.

Table 1: *Photophysical properties of* ***1a-2b*** *in MeCN before and after degassing.*

	Before degassing					**After degassing**				
	Φ_{PL} (%)	λ_{max} (nm)	τ_e (μs)	k_r (s^{-1}) X 10^5	k_{nr} (s^{-1}) X10^6	Φ_{PL} (%)	λ_{max} (nm)	τ_e (μs)^a	k_r(s^{-1}) X 10^5	k_{nr} (s^{-1}) X 10^6
1a	0.6 ± 0.1	512	0.026	2.3± 0.4	38.2± 6.4	2.8 ± 0.3	512	0.09, 1.60	-	-
1b	0.9 ± 0.1	512	0.031	2.9± 0.3	32.0± 3.6	50.8 ± 4.0	510	1.90	2.7 ± 0.2	0.26 ± 0.02
2a	1.0 ± 0.1	468, 495	0.040	2.5± 0.3	24.8± 2.5	1.7 ± 0.2	462, 510	0.11, 0.98	-	-
2b	1.2 ± 0.1	470, 497	0.047	2.6± 0.2	21.0± 1.8	65.6 ± 5.0	470, 496	2.60	2.5 ± 0.2	0.13 ± 0.01

[a] See ESI for details of bi-exponential decay processes in **1a** and **2a**.

Results and discussion

Photophysical characterisation

The complexes under study are based on gpy N^N ligands,[21] which are strongly donating compared to traditional diimine ligands such as 2,2′-bipyridine and coordinate to a wide variety of metal ions,[20,22-25] including iridium (**Fig. 1**).[18] Complexes **1a,b–2a,b** were prepared in 71–-81% yield. The desired complexes were synthesised by allowing one equivalent of Ir dimer, $[Ir(C^\wedge N)_2Cl]_2$ to react with a gpy ligand containing a CF_3 group, gpy-CF_3, (**1a** and **2a**) or a CH_3 group, gpy-Me, (**1b** and **2b**).

The photophysical properties of these four complexes were measured in both aerated and degassed MeCN. The photoluminescence (PL) spectra in aerated solution are shown in **Fig. 2(a)** while the PL decay traces are shown in **Fig. 2(b)**; Φ_{PL} values, PL lifetime (τ_e) and calculated radiative (k_r) and non-radiative decay (k_{nr}) rate constants are given in **Table 1**. The analysis shows that all four complexes have similar respective Φ_{PL}, k_r and k_{nr} prior to degassing.

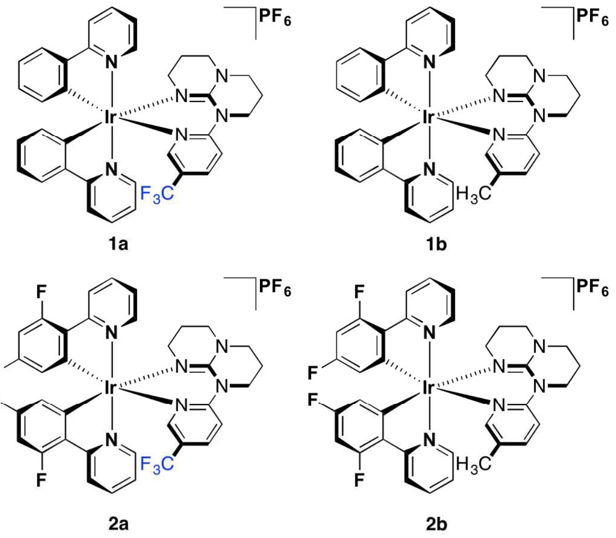

1a 1b

2a 2b

Figure 1: Complexes under investigation in this study.

Upon degassing the solutions, a dramatic divergence in photophysical behaviour is observed between **1a**/**2a** and **1b**/**2b**. The Φ_{PL} values are more than 50% for **1b** and **2b**, but remain around 2% for **1a** and **2a**. The PL decays for **1b** and **2b** are monoexponential, with τ_e ~ 2 μs (**Fig. 3** and **Table S1**), typical for cationic iridium complexes.[26-28] By contrast, the PL decays of **1a** and **2a** are biexponential, with the average τ_e < 300 ns (**Fig. 3** and **Table S1**). Upon degassing, k_r shows essentially no net change for **1b/2b**, while k_{nr} decreases by two orders of magnitude. We attribute the low Φ_{PL} values observed for **1a** and **2a** to strong vibrational coupling[10,14,16] principally among the asymmetric stretching modes of the Ir-N_{dFppy} bonds and the asymmetric stretching modes of the C-N and C-C bonds of the pyridine ring of the CF_3-gpy in **1a** and **2a**.

This hypothesis is corroborated by DFT calculations where the LUMO (lowest unoccupied molecular orbital) is switched from the CF_3-gpy moiety in **2a** to the pyridine unit of the C^N ligands in **2b** (**Fig. 4**); a similar relationship exists for **1a/1b** (**Fig. S20**). With the presence of more electron-withdrawing fluoro substituents, the emission profiles of complexes **2a** and **2b** are expectedly blue-shifted compared to those of **1a** and **1b**. The emission spectra of **1a** and **1b** are broad and featureless, indicative of a mixed ^{3}CT emission while the spectra of **2a** and **2b** are structured, suggesting a significant ^{3}LC-based emission. Unrestricted DFT calculations support this assignment as they show the triplet state spin density is principally localised on both the Ir(III) centre and the C^N ligands for all complexes, but to some extent is also delocalised onto the guanidyl part of the ancillary CH_3-/CF_3-gpy ligand in complexes **1a** and **1b**, which is not the case for complexes **2a** and **2b** (Fig. **5**).

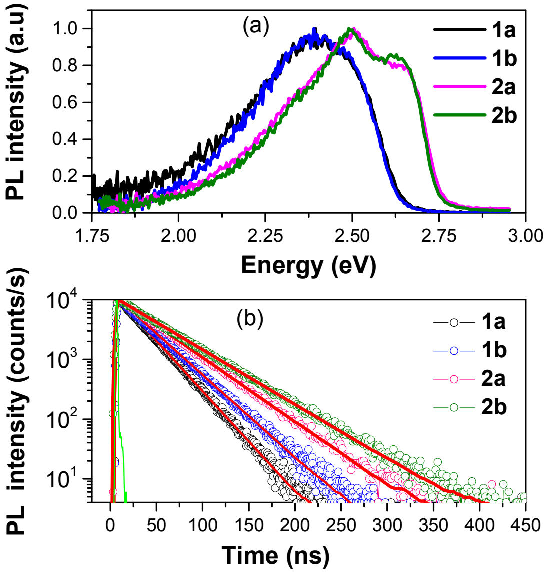

Figure 2: Emission spectra of **1a–2b** in MeCN in air (λ_{exc} = 360 nm). (b) Photoluminescence decay of **1a–2b** in MeCN in air (λ_{exc} = 375 nm). The experimental data was fitted to a monoexponential decay (red lines).

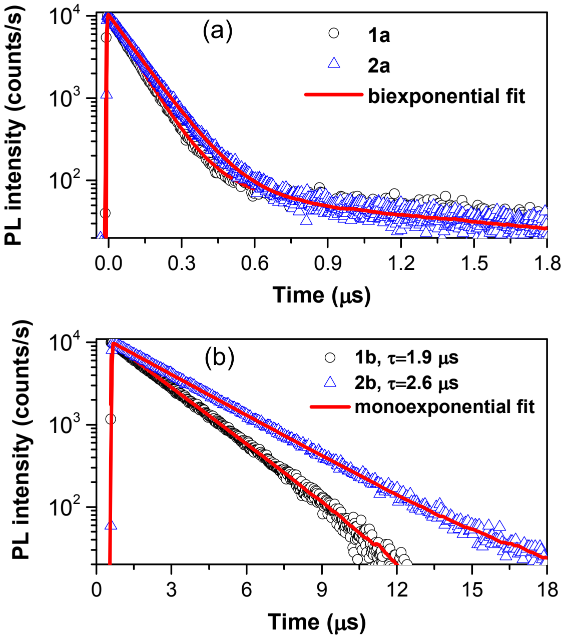

Figure 3: Photoluminescence decay of (a) **1a** and **2a** and (b) **1b** and **2b** in degassed MeCN solution. λ_{exc} = 375 nm. fits are shown in red.

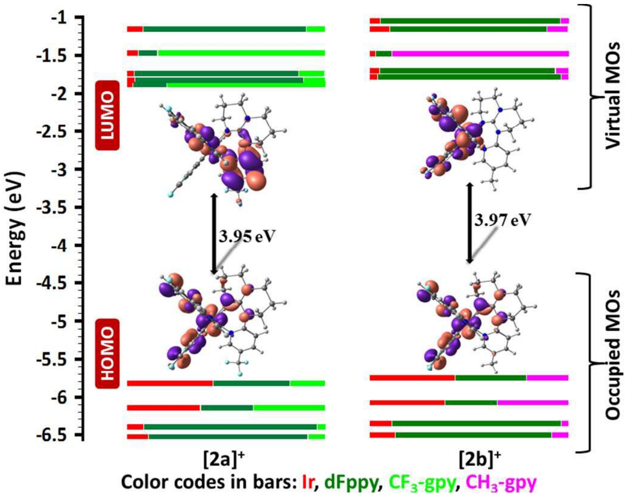

Figure 4: Calculated frontier MO energies of [**2a**]$^+$ and [**2b**]$^+$, obtained from DFT [(B3LYP/SBKJC-VDZ for Ir(III)) and (6-31g** for C,H,N,F] with CPCM(CH_3CN) and 0.5 eV threshold of degeneracy (isovalued at 0.03). Kohn-Sham MOs of [**2a**]$^+$ and [**2b**]$^+$ are also shown.

Frequency calculations suggest that there is a strong coupling among the asymmetric stretching modes of the Ir-N_{dFppy} bonds and the asymmetric stretching modes of the C-N and C-C bonds of the pyridine ring of the CF_3-gpy ligand in **2a** (vibrational mode #121, E = 1054 cm^{-1}) (see **Table S4** for other minor contributing vibrational modes that couple with the spin density). This coupling is found to be very weakly present in **2b**, the analog complex containing CH_3-gpy. Thus, the strong vibrational coupling present in the T_1 state leads to poor Φ_{PL} for **2a** (**1a**) and not for **2b** (**1b**).

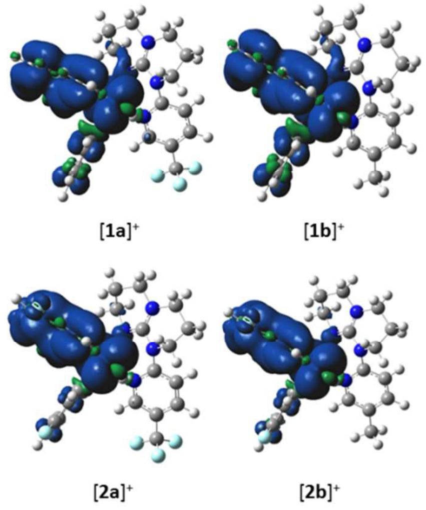

Figure 5. Triplet spin density distributions of complexes [**1a**]$^+$, [**1b**]$^+$, [**2a**]$^+$ and [**2b**]$^+$, obtained from TD-DFT [(UB3LYP/SBKJC-VDZ for Ir(III)) and (6-31g** for C,H,N,F] with CPCM(MeCN) (isovalue at 0.02).

This vibrational coupling can be quantified by analysis of the Huang-Rhys factors which were estimated from the relative strength of (0,1) and (0,0) transitions. Complexes **2a** and **2b** have well-defined 0–0 and 0–1 peaks in their degassed PL spectra while this is not the case for **1a** and **1b**. Therefore, we used **2a** and **2b** to further investigate the nature of this vibrational coupling. From the analysis there is stronger vibrational coupling in **2a** (Huang Rhys factor = 1.14) compared to **2b** (Huang Rhys factor = 1.09).

For electroluminescence applications, an emitter with a high Φ_{PL} in the solid state is required. Previously it has been shown that the Φ_{PL} can be improved by blending the emissive complex within an inert solid host.[14,29] Therefore, we blended our complexes with PMMA to modulate the vibrational coupling in order to enhance the emission efficiency of the complexes. The photophysical data is shown in **Table S3** (ESI). Both **2a** and **2b** show relatively high Φ_{PL} in thin film, with a notable recovery of Φ_{PL} for **2a** measured in air (> 65%) and under an N_2 environment (> 72%) given that **2a** was only slightly emissive (1.7%) in degassed solution.

We undertook temperature-dependent photophysical studies in order to comprehend further the contrasting behaviour of **2a** in solution and thin film. A comparison of the PL emission of 2 wt% **2a** in PMMA at room temperature and at 77 K (λ_{exc} = 380 nm) is shown in **Fig. 6(a)**. It can be seen that the 0-0 and 0-1 peaks are more prominent in the solid-state spectrum at room temperature compared to the degassed MeCN solution spectrum (**Fig. S18(b)**). This shows that having the complex embedded in the host PMMA inhibits significantly the vibrational coupling of the CF_3-moiety associated with the non-radiative decay of the PL emission. At 77 K the 0–0 peak becomes even more prominent (Huang Rhys factor = 1.05) due to reduced vibrational coupling compared to the measurements at 300 K (Huang Rhys factor = 1.15) and in MeCN degassed solution spectra (Huang Rhys factor = 1.14). Moreover, relative intensity of PL emission increases at 77 K.

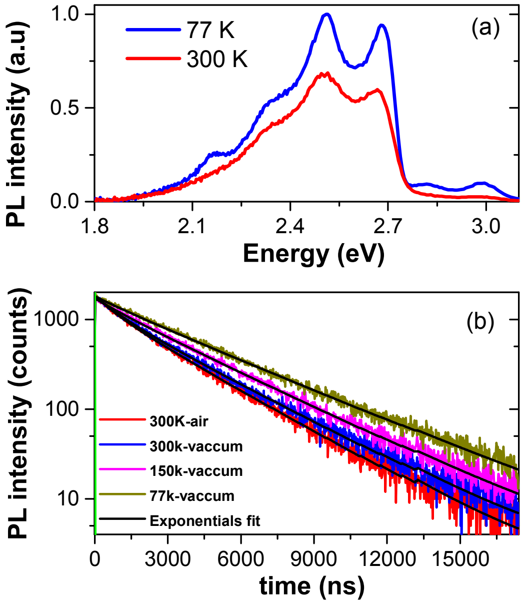

Figure 6: (a) PL spectra of 2 wt% **2a** in PMMA measured at 300 K and 77 K (λ_{exc} = 380 nm). (b) Temperature-dependent PL decay of 2 wt% **2a** in PMMA measured in air and under vacuum (λ_{exc} = 379 nm) with fits shown in black.

The transient PL decays of 2 wt% **2a** in PMMA at different temperatures and in different environments (air and vacuum) are shown in **Fig. 6(b)** and the photophysical data collected in **Table 2** and **Table S2**. Both components of the decay of **2a** under vacuum are longer-lived than under air due to the absence of O_2, which quenches phosphorescence. The τ_e increases upon cooling, to 3.2 µs at 150 K and 3.7 µs at 77 K due to suppression of thermally-activated non-radiative processes,[15] including the coupling of the excited state to vibrational modes. Furthermore, the lifetime measured in the solid state is more than 15 times longer than that in degassed MeCN. This shows that doping **2a** into PMMA significantly reduces the vibrational quenching at room temperature and this vibrational quenching is almost completely absent at 77 K.

Table 2: *Photophysical properties of* ***2a*** *in DCM and 2 wt% of* ***2a*** *in PMMA thin film* measured at room temperature (300 K)

2a	DCM		Film	
	Before degassing	After degassing	Air	Vacuum
Φ_{PL} (%)	1.0	1.7	65.9	72.4
τ_e (µs)[a]	0.04	0.11, 0.98	0.82, 2.80	0.92, 3.00

[a] See ESI for details of bi-exponential decay processes.

Device fabrication

After controlling the vibrational coupling in the solid state, we investigated the electroluminescence of **2a** and **2b** by fabricating solution-processed organic light emitting diodes (OLEDs). For comparison, we also fabricated OLEDs with **1b**. The device architecture consisted of following layers: ITO / PEDOT:PSS (30 nm) / PVK (30 nm) / mCP:OXD7:**1b**–**2b**(75:20:5 wt%) (30 nm) / B3PYMPM (60 nm) / Ca (20 nm) / Al (100 nm). Here poly(3,4-ethylenedioxythiophene):poly(styrene sulfonate) (PEDOT:PSS) is the hole injection layer and was spin-coated at 4000 rpm for 60 s and then baked at 120 ^{0}C for 20 minutes to obtain a 35 nm smooth film. Poly(*N*-vinylcarbazole) (PVK) was used as the hole transporting layer. PVK was spin-coated from chlorobenzene at 2000 rpm inside the nitrogen-filled glovebox. It was then baked at 80 ^{0}C for 2h to form a smooth film of 30 nm thickness. The emitting layer consisted of 1,3-bis(*N*-carbazolyl)benzene (mCP) and 2,2′-(1,2-phenylene)bis[5-(4-*tert*-butylphenyl)-1,3,4-oxadiazole] (OXD-7) as host materials and phosphorescent dopants **1b**–**2b**, which were cast from acetonitrile at 2000 rpm to form a film of 30 nm thickness. OXD7 and mCP are wide band gap (3.7 eV) materials.[30, 31] OXD7 and mCP were selected because they are wide band gap materials with high triplet energies and together can transport both electron and hole well. A 60 nm electron-transporting layer 4,6-bis(3,5-di(pyridin-3-yl)phenyl)-2-methylpyrimidine (B3PyMPM) was then thermally evaporated onto the emitting layer under high vacuum. Finally, the composite cathode Ca (20 nm) / Al (100 nm) was thermally deposited through a shadow mask in the vacuum chamber at ~ 2.0×10^{-6} mbar. The device architecture along with the energy levels are shown in **Fig. 7**. The electroluminescence (EL) spectra of the three devices are shown in **Fig. 8(a)**. EL spectra of **2a** and **2b** are similar to their PL spectra but are red-shifted and show different relative intensities of the vibronic peaks. However, the EL spectrum of **1b** has two distinct vibronic peaks compared to PL spectra, which showed only one broad peak, pointing to a greater ligand-centered character to the emission of **1b** in the device. In the EL spectra, we did not observe any emission around 410 nm (expected emission from host) due to complete energy transfer from the host to the iridium emitters.[32] Current-voltage characteristics of the devices are shown in **Fig. 8(b)**.

(a)

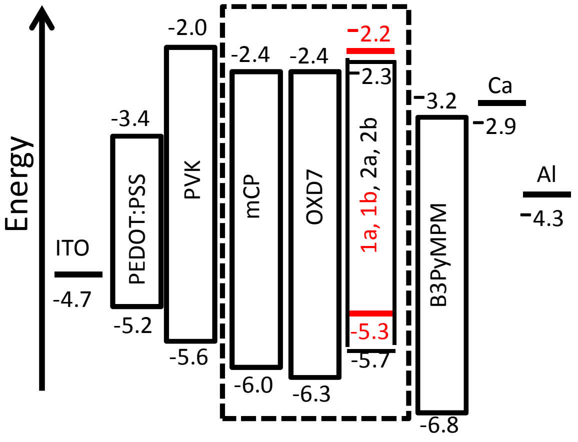

(b)

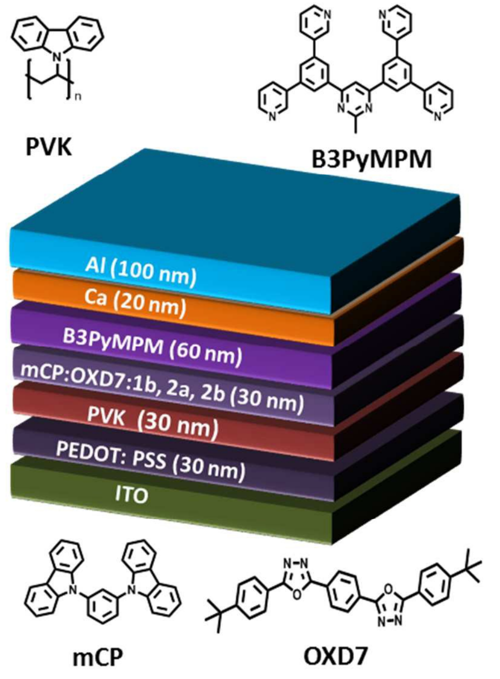

Figure 7: (a) Energy level diagram of light emitting devices using **1b–2b** as the emitter. (b) Schematic of fabricated light emitting devices fabricated using **1b-2b**.

The device made from **1b** showed the highest current density at high voltage (> 6 V), followed by the devices with **2b** then **2a**. The turn-on voltage for the OLED with **2a** is lower than that with **2b**.

All devices show a steep increase in luminance with voltage once turned on (see **Fig. 8(c)**). A maximum luminance of 1846 cd/m^2 at a driving voltage of 10 V, 881 cd/m^2 at 15.1 V and 332 cd/m^2 at 15.1 V was achieved for **1b**, **2a** and **2b**, respectively. The luminance characteristics of the devices (Fig. **8 (c)**) show that the OLED based on **1b** has the lowest turn-on voltage and highest power and current efficiencies among all devices whereas **2b** has the highest turn-on voltage. The external quantum efficiencies (EQE) of the devices are given in **Fig. 8(d)**. The EL properties are summarized in **Table 3**.

The maximum EQE of 6.5% was obtained for **1b** at a luminance of 41 cd/m^2 (7V), which reduced only slightly to 6.3% at 100 Cd/m^2 and 5.8% at 1000 Cd/m^2. A similar low roll off of the EQE for **2a** and **2b** was also observed. A maximum EQE of 2.4% at luminance of 35 cd/m^2 was obtained for **2a**, which reduced to 2.3% at 100 Cd/m^2, whereas in the case of **2b**, a maximum EQE of 3.0% was obtained at 40 cd/m^2, which reduced to 2.8% at 100 Cd/m^2.

The EQE of 6.3% and current efficiency of 20.8 Cd/m^2 at a luminance of 100 cd/m^2 for **1b** is among the best performing OLEDs based on the use of cationic iridium complexes as emissive layer.[33-39] To the best of our knowledge the best performing solution-processed device using a cationic iridium complex as the emitter showed a maximum EQE of 7.1% and CE of 10.0 cd/m^2.[39] This device used [Ir(npy)$_2$(c-phen)]PF$_6$, (npy is 2-(naphthalen-1-yl)pyridinato c-phen = 1-Ethyl-2-(9-(2-ethylhexyl)-9*H*-carbazol-3-yl)-1*H*-imidazo[4,5-f][1,10]phenanthroline). Due to the use of strongly conjugated C^N ligands the emission colour of the device was in the red region with CIE coordinates of (0.57, 0.40)[39] and so a direct comparison to the current devices is not appropriate. Recently, Duan and co-workers reported the use of the blue-green [Ir(ppy)$_2$(pzpy)][PF$_6$] (pzpy = 2-(1Hpyrazol-1-yl)pyridine) complex as the emitter in a a single-layer solution-processed OLED.[40] A maximum EQE of 6.8% with current efficiency of 17.1 cd/m^2 was obtained with CIE coordinates of (0.21, 0.48).

Table 3: *Electroluminescence characteristics of the OLEDs.*

Emitter	V_{on}[a] (V)	λ_{peak}[b] (nm)	EQE[c] (%)	CE[d] (cd/A)	PE[e] (lm/W)	CIE[f]
1b	5.8	527	6.3	20.8	8.7	(0.29, 0.58)
2a	6.3	506	2.3	6.2	1.9	(0.26, 0.47)
2b	7.8	503	2.8	7.1	1.6	(0.22,0.43)

[a] Turn-on voltage @ 1 cd/m^2. [b] Peak wavelength at 1 mA/cm^2. [c] External quantum efficiency at 100 cd/m^2. [d] Current efficiency at 100 cd/m^2. [e] Power efficiency at 100 cd/m^2. [f] The Commission Internationale de L'Eclairage (CIE) coordinates at 1 mA/cm^2.

Our device using **1b** has CIE coordinates of (0.29, 0.58) and so is slightly red-shifted and has a slightly higher current efficiency compared to the device of Duan *et al.* The device with **1b** exhibits considerably better performance. We attribute this to the shallower HOMO enabling more efficient hole injection, which explains the lower turn-on voltage and improved charge balance and device efficiency. The device with **2a** has the lowest EQE, despite a higher luminance and similar power efficiency compared to **2b** (**Fig. 8(d)** and **8 (e)**). These results suggest there may be poorer charge carrier balance in these devices.[17, 32, 41]

Conclusions

In summary, we have shown that the suppressed emission of CF$_3$-containing complexes **1a** and **2a** in MeCN solution can be overcome by decreasing the temperature or by embedding these complexes in a rigid PMMA matrix. In fact, emission in the thin film is enhanced by ca. 30-fold compared to measurement in degassed solution. The supressed emission in solution is the result of strong coupling of the excited state to vibrational modes implicating the CF$_3$-group; whereas **1a** and **2a** show Φ_{PL} of <1%, replacement of the CF$_3$- group by CH$_3$- recovers the emission without affecting the emission energy, with Φ_{PL} >50%. OLEDs were made with both solution-state emissive (**2b**) and non-emissive complexes (**2a**). Their performance resulted in similar EQEs measured for both devices. Thus, this study demonstrates the importance of assessing the solid-state optoelectronic properties of emitters prior to their considered use in EL devices.

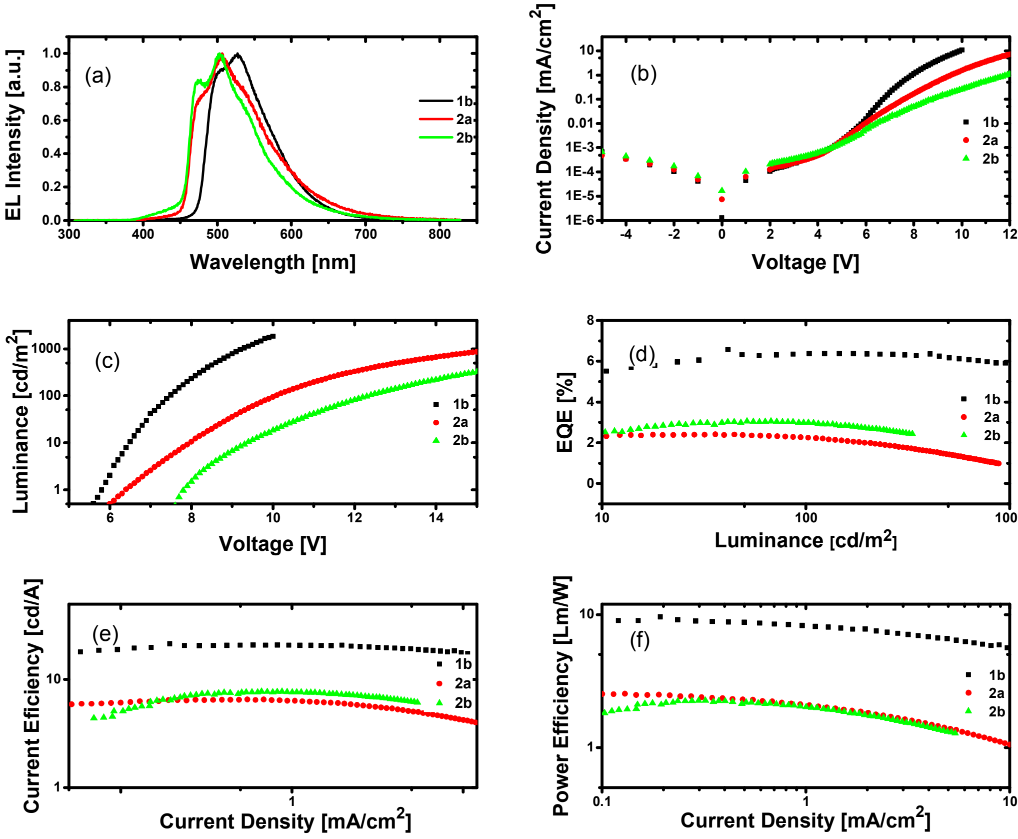

Figure 8. (a) EL spectra of three complexes. (b) Current density of **1b** (black), **2a** (red) and **2b** (green) as function of voltage of OLEDs. (c) Luminance as a function of applied voltage. (d) External quantum efficiency (EQE) as a function of Luminance. (e) Current efficiency as a function of current density. (f) Power efficiency as a function of current density for the devices fabricated using **1b**, **2a** and **2b**.

Acknowledgements

We are grateful to the European Research Council (grant 321305), EPSRC (grants EP/J01771X, EP/L017008/1 and EP/M02105X/1) for financial support. IDWS acknowledges a Royal Society Wolfson Research Merit Award. GSH thanks the Natural Sciences and Engineering Research Council (NSERC) of Canada for funding.

Notes and references

1. Y. You and S. Y. Park, *Dalton Trans.*, 2009, 1267-1282.
2. L. Xiao, Z. Chen, B. Qu, J. Luo, S. Kong, Q. Gong and J. Kido, *Adv. Mater.*, 2011, **23**, 926-952.
3. H. Xu, R. Chen, Q. Sun, W. Lai, Q. Su, W. Huang and X. Liu, *Chem. Soc. Rev.*, 2014, **43**, 3259-3302.
4. R. D. Costa, E. Ortí, H. J. Bolink, F. Monti, G. Accorsi and N. Armaroli, *Angew. Chem. Int. Ed.*, 2012, **51**, 8178-8211.
5. T. Hu, L. He, L. Duan and Y. Qiu, *J. Mater. Chem.*, 2012, **22**, 4206-4215.
6. M. S. Lowry and S. Bernhard, *Chem. Eur. J.*, 2006, **12**, 7970-7977.
7. A. F. Henwood and E. Zysman-Colman, *Top. Curr. Chem.*, 2016, **374**, 1-41.
8. S. Ladouceur and E. Zysman-Colman, *Eur. J. Inorg. Chem.*, 2013, **2013**, 2985-3007.
9. M. A. Baldo, D. O'brien, Y. You, A. Shoustikov, S. Sibley, M. Thompson and S. Forrest, *Nature*, 1998, **395**, 151-154.
10. S.-C. Lo, R. E. Harding, C. P. Shipley, S. G. Stevenson, P. L. Burn and I. D. Samuel, *J. Am. Chem. Soc.*, 2009, **131**, 16681-16688.
11. M. Baldo, M. Thompson and S. Forrest, *Nature*, 2000, **403**, 750-753.

12. X. Gong, W. Ma, J. C. Ostrowski, G. C. Bazan, D. Moses and A. J. Heeger, *Adv. Mater.*, 2004, **16**, 615-619.
13. C. Adachi, M. A. Baldo, M. E. Thompson and S. R. Forrest, *J. Appl. Phys.*, 2001, **90**, 5048-5051.
14. R. E. Harding, S.-C. Lo, P. L. Burn and I. D. Samuel, *Org. Electron.*, 2008, **9**, 377-384.
15. T. Sajoto, P. I. Djurovich, A. B. Tamayo, J. Oxgaard, W. A. Goddard III and M. E. Thompson, *J. Am. Chem. Soc.*, 2009, **131**, 9813-9822.
16. J. A. Treadway, B. Loeb, R. Lopez, P. A. Anderson, F. R. Keene and T. J. Meyer, *Inorg. Chem.*, 1996, **35**, 2242-2246.
17. J. Lee, H.-F. Chen, T. Batagoda, C. Coburn, P. I. Djurovich, M. E. Thompson and S. R. Forrest, *Nat. Mater.*, 2016, **15**, 92-98.
18. K. Hasan, A. K. Pal, T. Auvray, E. Zysman-Colman and G. S. Hanan, *Chem. Commun.*, 2015, **51**, 14060-14063.
19. M. Nonoyama, *Bull. Chem. Soc. Jpn.*, 1974, **47**, 767-768.
20. A. K. Pal, S. Nag, J. G. Ferreira, V. Brochery, G. La Ganga, A. Santoro, S. Serroni, S. Campagna and G. S. Hanan, *Inorg. Chem.*, 2014, **53**, 1679-1689.
21. A. K. Pal, P. K. Mandali, D. K. Chand and G. S. Hanan, *Synlett*, 2015, **26**, 1408-1412.
22. S. Nag, J. G. Ferreira, L. Chenneberg, P. D. Ducharme, G. S. Hanan, G. La Ganga, S. Serroni and S. Campagna, *Inorg. Chem.*, 2010, **50**, 7-9.
23. A. K. Pal, P. D. Ducharme and G. S. Hanan, *Chem. Commun.*, 2014, **50**, 3303-3305.
24. A. K. Pal, S. Serroni, N. Zaccheroni, S. Campagna and G. S. Hanan, *Chem. Sci.*, 2014, **5**, 4800-4811.
25. A. K. Pal, N. Zaccheroni, S. Campagna and G. S. Hanan, *Chem. Commun.*, 2014, **50**, 6846-6849.
26. S. Ladouceur, D. Fortin and E. Zysman-Colman, *Inorg. Chem.*, 2011, **50**, 11514-11526.
27. L. He, L. Duan, J. Qiao, R. Wang, P. Wei, L. Wang and Y. Qiu, *Adv. Funct. Mater.*, 2008, **18**, 2123-2131.
28. R. D. Costa, E. Ortí, H. J. Bolink, S. Graber, S. Schaffner, M. Neuburger, C. E. Housecroft and E. C. Constable, *Adv. Funct. Mater.*, 2009, **19**, 3456-3463.
29. T. Sajoto, P. I. Djurovich, A. Tamayo, M. Yousufuddin, R. Bau, M. E. Thompson, R. J. Holmes and S. R. Forrest, *Inorg. Chem.*, 2005, **44**, 7992-8003.
30. D. O'Brien, A. Bleyer, D. Lidzey, D. Bradley and T. Tsutsui, *J. appl. Phys.*, 1997, **82**, 2662-2670.
31. K. Masui, H. Nakanotani and C. Adachi, *Org. Electron.*, 2013, **14**, 2721-2726.
32. A. F. Henwood, A. K. Bansal, D. B. Cordes, A. M. Slawin, I. D. Samuel and E. Zysman-Colman, *J. Mater. Chem. C*, 2016, **4**, 3726-3737
33. E. A. Plummer, A. van Dijken, J. Hofstraat, L. De Cola and K. Brunner, *Adv. Funct. Mater.*, 2005, **15**, 281-289.
34. W. Y. Wong, G. J. Zhou, X. M. Yu, H. S. Kwok and Z. Lin, *Adv. Funct. Mater.*, 2007, **17**, 315-323.
35. L. He, L. Duan, J. Qiao, D. Zhang, G. Dong, L. Wang and Y. Qiu, *Org. Electron.*, 2009, **10**, 152-157.
36. L. He, L. Duan, J. Qiao, D. Zhang, L. Wang and Y. Qiu, *Org.Electron.*, 2010, **11**, 1185-1191.
37. B. Park, Y. H. Huh, H. G. Jeon, C. H. Park, T. K. Kang, B. H. Kim and J. Park, *J. Appl. Phys.*, 2010, **108**, 094506.
38. G. Nasr, A. Guerlin, F. Dumur, L. Beouch, E. Dumas, G. Clavier, F. Miomandre, F. Goubard, D. Gigmes and D. Bertin, *Chem. Commun.*, 2011, **47**, 10698-10700.
39. H. Tang, Y. Li, B. Zhao, W. Yang, H. Wu and Y. Cao, *Org. Electron.*, 2012, **13**, 3211-3219.
40. D. Ma, C. Zhang, Y. Qiu and L. Duan, *J. Mater. Chem. C*, 2016, **4**, 5731-5738
41. M. Y. Wong, G. Xie, C. Tourbillon, M. Sandroni, D. B. Cordes, A. M. Slawin, I. D. Samuel and E. Zysman-Colman, *Dalton Trans.*, 2015, **44**, 8419-8432.